Polymer 55 (2014) 4150–4155

Contents lists available at ScienceDirect

Polymer

journal homepage: www.elsevier.com/locate/polymer

External normal pressure prevents preferential wetting of PS/PMMA blend thin films

Zheng Zhang, Zhen Wang, Yifu Ding*

Department of Mechanical Engineering, University of Colorado at Boulder, Boulder, CO 80309-0427, USA

ARTICLE INFO

Article history:
Received 22 April 2014
Received in revised form
19 May 2014
Accepted 8 June 2014
Available online 14 June 2014

Keywords:
Blend thin film
Wetting
Confinement effect

ABSTRACT

Substrate wetting of the component(s) of thin polymer blend films strongly dictates their phase evolution during thermal annealing. In the case of wetting by one component being preferential than the other, a continuous wetting layer at the substrate will form. Here, we report that the preferential wetting of PMMA within a PS/PMMA thin film can be prevented under normal pressure. Moreover, the external pressure drives the PMMA wetting layer at the substrate (or a PMMA cushion layer intentionally placed between the blend film and the superstrate) into the isolated PMMA domains within the blend film. This results in a film morphology normally observed on neutral surfaces, revealing that normal pressure can potentially be used to effectively control the blend film morphology by preventing the hydrodynamic wetting.

© 2014 Elsevier Ltd. All rights reserved.

1. Introduction

The phase structures of polymer blend thin films are important for diverse applications, ranging from organic photovoltaics [1], LEDs [2] to chemical sensors [3]. It has been shown that the "morphological evolution of thin blend film is a result of dynamic interplay among wetting, domain coarsening, capillary fluctuation, hydrodynamic flow and thin film confinement" [4]. Among them, the wetting of component(s) at the polymer–substrate interface has been found to be one particularly influential factor [5–7].

For a thin, binary blend film bounded by a rigid substrate that energetically favors one component to another, the preferential attraction drives the favored component to either "partially wet" or "completely wet" the substrate, depending on the degree of wettability [8]. In the complete wetting scenario, the substrate-favored phase is enriched at the interface and forms a *continuous* wetting layer, via either diffusion [9,10] or hydrodynamic flow [11]. When the wetting layer formation occurs during phase separation near the critical point, the growth kinetics follows a power law, $l \propto t^{\alpha}$, where the exponent α depends on the dominant growth mechanism [11].

The wetting layer separates the unfavored component from contacting the substrate, which greatly affects the domain-coarsening process [12]. For thin PS/PMMA [13,14] (or SAN/PMMA [11,15,16]) films, a well-studied system, complete wetting of PMMA on more hydrophilic surfaces (SiO_x, mica, etc.) were observed, which facilitated the coalescence of domains through hydrodynamic wetting.

When a thin blend film was symmetrically confined between two identical preferential walls, wetting layers formed on both sides [17,8], which indeed had been observed by measuring composition depth profile of a polyolefin blend film [18]. In relatively thick PS/PVME films (10 s–100 s μm) confined between two glass slides (preferential surface for PVME), the wetting layers could grow up to several micrometers thick, which served as the active path for hydrodynamic mass transport between PVME domains [19–21]. As noted by the author, this morphological evolution was length-scale-dependent, meaning that the thickness of the wetting layer limited the kinetics of the coalescence [22].

Efforts were also made in order to investigate the phase behaviors of symmetrically confined blend films in even thinner thickness range. Dalnoki-Veress et al. studied ultrathin PS/PMMA films (~100 nm in thickness), which had been capped with a thin evaporated SiO_x layer on one side and, on the other side, supported on a silicon substrate with a ~70 nm thick SiO_x layer. Wetting layers of PMMA also formed on both the superstrate and the substrate [23]. The thin top surface layer was not rigid enough (when thickness was below a certain threshold value) to suppress the film-roughening caused by domain-coarsening [23]. Consequently, the bending of the capping layer was observed, which caused the

* Corresponding author.
E-mail address: yifu.ding@colorado.edu (Y. Ding).

http://dx.doi.org/10.1016/j.polymer.2014.06.023
0032-3861/© 2014 Elsevier Ltd. All rights reserved.

geometrical configuration to deviate from perfect symmetry. In addition, a novel route to fabricating highly uniform polymer blend concentric rings were achieved by capping/confining an asymmetric blend between a spherical surface and a flat one [24].

The preferential wetting could be prevented by "neutralizing" the substrate surface energy. For PS/PMMA, the neutral surface could be achieved by surface assembled monolayer, random copolymer of styrene and methyl methacrylate, or even a mixture of PS/PMMA chains [25,26]. On these neutral surfaces, both PS and PMMA formed direct contact with the substrate, without any continuous wetting layer. This approach had been adopted for improving the ordering of block copolymers [27]. In the current study, we examined the morphological evolution of thin PS/PMMA blend films annealed while being confined between two identical rigid walls under a normal pressure. Most significantly, we found that the external pressure could not only completely prevent the formation of a PMMA wetting layer, but also drive an existing wetting layer into isolated PMMA domains. As a result, direct contact of both PS and PMMA domains with both capping substrates, in a way similar to what had been observed on neutral surfaces, were achieved.

2. Experimental

Polystyrene "PS48k" (Molecular weight M_w = 48.1 kg/mol, Polydispersity Index M_w/M_n = 1.01, Glass transition temperature T_g = 98 °C) and poly(methyl methacrylate) "PMMA15k" (Approximately M_w = 15 kg/mol, as determined by GPC, T_g = 105 °C) were purchased from Scientific Polymer Products, Inc. and used as received. Both polymers were dissolved with a concentration ratio of 1:1 in toluene at room temperature.

PS48k/PMMA15k blend films with different thicknesses were prepared by spin-casting blend solutions of different concentrations onto silicon wafers at 2000 rpm. The surfaces of the wafers had been previously cleaned with oxygen plasma. The as-cast films were annealed *in vacuo* at 50 °C (below the T_g of both polymers) for 8 h in order to remove residual solvent [28]. The thickness of the as-cast films was determined by measuring the step-height of a razor blade scratch on the films with atomic force microscopy (AFM, Dimension 3100, Bruker Corporation).

In order to achieve symmetrical boundary conditions, an identical silicon wafer with native oxide surface was pressed (under a normal pressure of 4 MPa) against the blend films at 110 °C for 60 s and then cooled down to room temperature, using an Eitre 3 nanoimprinter (Obducat, Inc.). The heated pressurization was crucial for achieving excellent contact and strong physical adhesion between the superstrate and the blend film. Since the temperature used for the pressurization was close to the T_gs of the PS and PMMA, no morphological change was expected for the brief period of heating.

For annealing without pressure (either capped or uncapped), the blend films were annealed on an STC200 hot-stage (Instec, Inc.) with a temperature stability of ±0.1 °C. The hot-stage had been calibrated with 7 melting-point standards prior to the annealing experiments. The pressurized annealing experiments were carried out using nanoimprint lithography (NIL). A pressure of 4 MPa was exerted as soon as the temperature ramped up to the annealing temperature. After 30 min, the temperature ramped down via air cooling, while the pressure was maintained at 4 MPa until room temperature was reached. In order to characterize the blend morphology, the capping silicon wafer and the blend film was separated by inserting a razor blade in between under room temperature.

The surface morphologies were characterized with AFM and optical microscopy. The PS/PMMA interfacial topography was measured with AFM after the selective dissolution of PS using cyclohexane. ImageJ 1.46r (Wayne Rasband, NIH) was used to process the power spectrum density profiles, extract the correlation lengths and calculate surface areas occupied by each phase.

3. Results and discussion

Fig. 1 (a–c) show AFM phase images of a 134 nm thick PS48k/PMMA15k blend film on Si substrate with a SiO_x surface, before and after having been annealed in air. The brighter (darker) regions were identified to be PMMA (PS) domains, respectively, and verified by selective dissolution of PS (Fig. 1 in Supporting Information). In the as-cast film, PMMA domains appeared isolated but highly correlated with a correlation wavelength of ~0.72 μm, while the PS domain formed the continuous matrix, as shown in Fig. 1(a). The inset of Fig. 1(a) further shows the PMMA domains were elevated, compared with the PS domains, which was attributed to the relatively higher solubility of PS in toluene [29]. As verified with AFM after selective etching of PS and schematically shown in Fig. 1(d), the more wettable component PMMA formed a continuous wetting layer at the blend–substrate interface, consistent with previous experiments [13,26]. This system falls into the "complete wetting" scenario [22]. Such as-cast morphology was caused by the spontaneous phase separation of PS/PMMA thin films and solvent evaporation during spin-coating [30,31].

The as-cast structure was non-equilibrium in nature, and would evolve towards the minimization of interfacial/surface energies once the polymers became mobile upon heating [13,29]. After annealing at 160 °C for 5 min, the PMMA domains started to round up and coarsen into bigger domains (Fig. 1(b)). This was driven by the Laplace pressure at the elevated PMMA/air interface, as indicated by the arrows in Fig. 1(d). As PMMA domains leveled, the adjacent PS domains coalescence together. At 30 min, PS had evolved from a continuous matrix into isolated droplets that are suspended on the PMMA matrix. (Fig. 1(c) and (d)). The PS domains took on rounded droplet shape due to interfacial-tension-driven shape relaxation [21] and the equilibrium of the contact angle between PMMA and air [32]. The correlation wavelength had increased to 7.5 μm. This lateral domain coalescence resulted in the root mean square (RMS) roughness of the film surface to increase to 113 nm, from 4.3 nm in the as-cast state. In the final morphology (Fig. 1(c)), the PS domains evolved from an apparent continuous phase into elevated and isolated droplets. We hereby refer to this process as "phase-inversion" [33]. The overall morphological evolution on a PMMA-preferred substrate was consistent with literature reports [29,31]. Such film roughening and phase inversion of PS/PMMA film can be prevented by using a neutral surface [13].

Next, we examined the morphological evolution of the same 134 nm blend film annealed under the confinement of two identical Si wafers but without external normal pressure. Simply placing a wafer on top of a PS/PMMA film would not form conformal contact. In this work, we used NIL to sandwich the PS/PMMA films between two identical Si wafers with SiO_x surfaces. Using the air-cushion method, NIL provided uniform pressure (<1% variation across a 3 inch wafer scale) and heating, which was critical for avoiding lateral shear in the blend films.

Fig. 1(e) shows the morphology of the film capped using NIL and then immediately separated. No significant difference in the domain size or distribution was found in the phase (comparing Fig. 1(e) with a)), which was ensured by the parameters used for capping (see Experimental). The corresponding height image shows a significant suppression in the surface topography (see inset of Fig. 1(e)). The overall roughness after capping was reduced to less than 2 nm.

After annealing, we observed *identical* morphologies on both the substrate side and the superstrate side. Here we present the

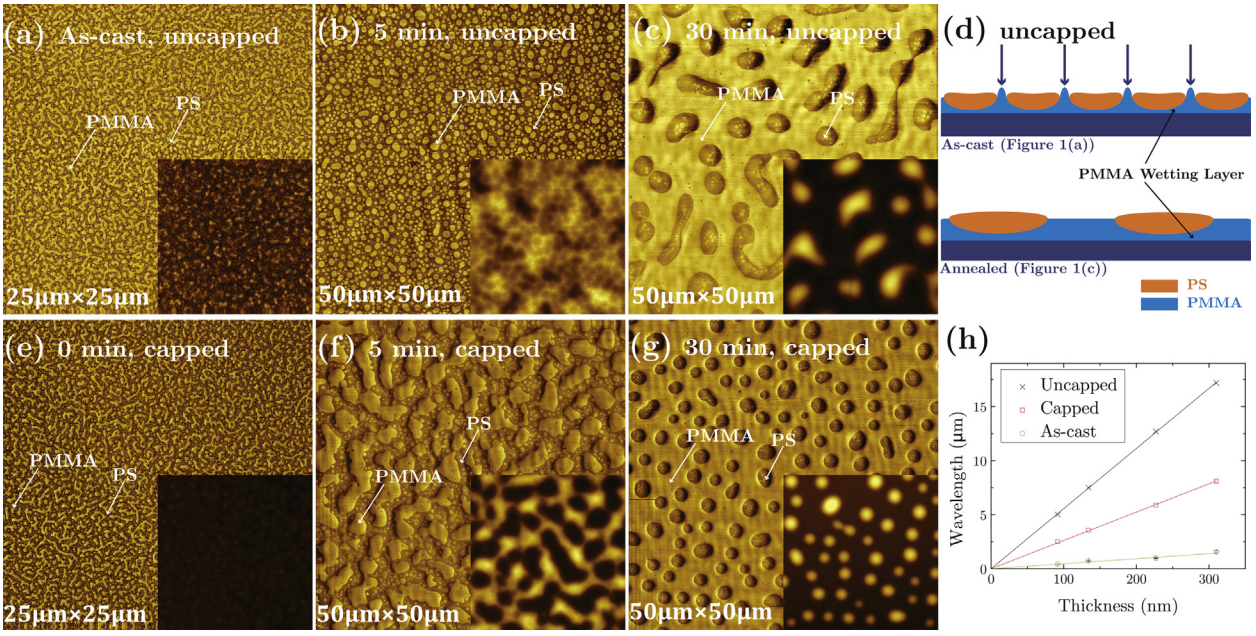

Fig. 1. (a–c) AFM phase images of a 134 nm thick PS48k/PMMA15k blend film annealed at 160 °C with the top surface exposed to air. (d) Cross-sectional schematics of the as-cast morphology and the annealed morphology. Arrows in (d) are simplified indication of Laplace pressure. (e–g) AFM phase images of the same PS48k/PMMA15k blend film confined between two identical wafers and annealed at 160 °C without pressurization. The colors in the phase images indicate material contrast, with the PMMA domains being brighter and the PS domains being darker. The annealing durations are indicated at the upper left corner of each image. Insets are the topographic images of the corresponding regions. (h) The wavelength of phase structure correlation as a function of initial film thickness in the as-cast film and the final annealed morphology for both uncapped and capped setup. The error bar represents the standard deviation in 5 randomly chosen areas. (For interpretation of the references to color in this figure legend, the reader is referred to the web version of this article.)

representative morphologies on the substrate side in Fig. 1(f) and (g). The figures evidently show the coalescence, preferential wetting of PMMA, film roughening, as well as the phase inversion, during subsequent annealing. All of these phenomena were qualitatively similar to the uncapped case. In the final morphology of Fig. 1(g), a ~20 nm wetting layer of PMMA was found on both the supstrate side and superstrate side, as determined from a scratch test on AFM. Though the exact pathway through which the PMMA migrated to the top superstrate is yet unclear, this process was evidently due to preferential wetting. The correlation lengths of the PS domains were around half of that obtained while annealing in open area (Fig. 1(h)), for all the different thicknesses examined.

The aforementioned morphological evolution was consistent with Tanaka's symmetrically confined micron-thick blend films, which was driven by the "wetting pressure" generated from the lateral curvature of the PMMA domains [22]. Hypothetically, the wetting pressure can be counter-balanced with an external normal pressure. Here we verify this hypothesis by annealing in the nanoimprinter pressurized chamber. The cross-sectional geometry of the sample is schematically shown in Fig. 2(d). Fig. 2(a) presents the phase evolution of a symmetrically capped PS48K/PMMA15K film with thickness ~130 nm annealed at 160 °C for 30 min under an external pressure of 4 MPa. Evidently, PMMA remained as the dispersed domains after the annealing, and PS remained the continuous phase. In other words, phase-inversion process, as observed in Fig. 1, did not occur during the pressurized annealing.

In addition, no PMMA wetting layer was found in the final morphologies by measuring the scratch step on the film using the AFM. The domain height of PMMA in Fig. 2(a) was ~130 nm, identical to the original thickness of the as-cast film, h_0. From volume conservation perspective, this equality affirms the non-existence of neither PMMA wetting layer nor PS wetting layer. This striking fact suggests that the external pressure applied on both sides of the wafers during the imprinting process not only hindered the PMMA wetting layer growth but also eliminated the existing thin wetting layer in the as-cast film (Fig. 1(d)), as schematically depicted in Fig. 2(d), by driving the PMMA flow from the wetting layer into the liquid vertical bridges.

It was without doubt that the kinetics of phase evolution would be hindered under compression. Therefore, it was necessary to examine the path of the morphological evolution. However, the NIL setup was not designed for extended duration of annealing. Instead, we annealed the PS/PMMA films under 190 °C and 210 °C for 30 min under 4 MPa, and the corresponding morphologies are shown in Fig. 2(b) and (c). Similar to that obtained at 160 °C, the films displayed a PMMA-dispersed morphology without any wetting layer. The PMMA domains occupied ~45% of the surface area. The average domain area of PMMA in each of the three samples was 0.76 μm^2, 5.7 μm^2 and 10.2 μm^2, respectively. The change in the average domain size reflected that the degree of PMMA domain coalescence, after the same amount of annealing time, evidently increased with the increase in temperature, due to the decreased viscosity of both PMMA and PS. Due to the lack of a mass transport layer, the coalescence of the PMMA domains in the pressurized films was most likely based upon collision. Note that in Fig. 2(c), PMMA domains in films annealed at 210 °C appeared more anisotropic than those observed at two other temperatures. This was most likely caused by the increased shape relaxation time (the time-scale for a PMMA domain to achieve circular shape, driven by the unbalanced in-plane Laplace pressure at the PS/PMMA interface) as the domains became larger.

Most significantly, the morphological evolution of sandwiched PS/PMMA films under pressure at all annealing temperatures were clearly different from previous blend films sandwiched under symmetrical wettable substrates without external pressure, where wetting layers on both substrates formed [17,22,23]. When a thick wetting layers forms, they can served as the active mass-transport path [19–22], in which case two major mechanisms are manifested

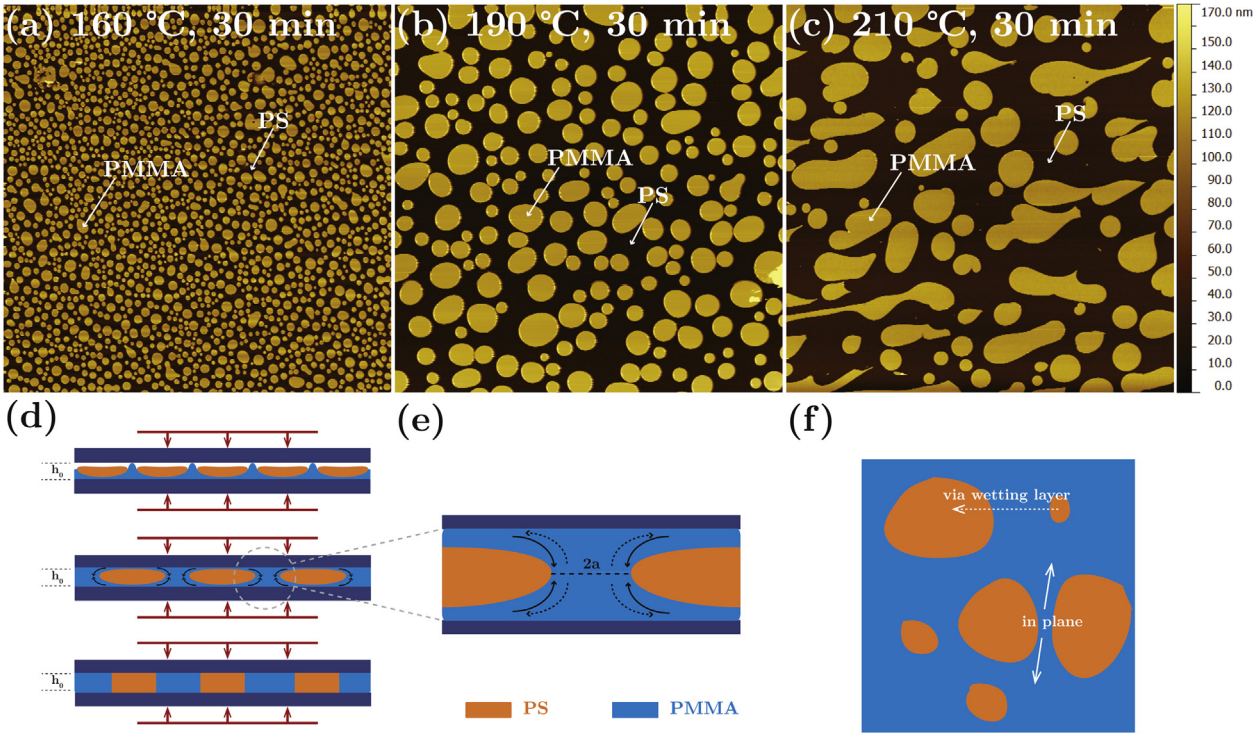

Fig. 2. (a–c) AFM height images of the 134 nm thick film under symmetrical confinement annealed at the labeled temperature for 30 min under 4 MPa and subsequent selective removal of PS. The scan size is 50 μm × 50 μm for all images. (d) Cross-sectional schematics of the evolution of phase structure under pressurized annealing and (e) the magnified view of the intermediate stage. (f) Top-down view of the coarsening process. This schematic is reproduced from Fig. 5 of Ref. [22].

in the coarsening process. In the lateral plane, two adjacent PMMA bridges can coarsen due to the capillary breakup of the PS in between, as indicated by the solid arrows in Fig. 2(f). In addition, the radial curvature of the PMMA liquid bridge that connects the two wetting layers exerts a wetting pressure that drives the mass into the wetting layer, represented by the dotted arrows in Fig. 2(e). Thus, a smaller liquid bridge shall coarsen into the bigger bridge, as mediated by the wetting layer, exerting a larger hydrodynamic pressure (dotted arrow in Fig. 2(f)). Denoting this radius of curvature as a in Fig. 2(e) and the interfacial tension between PS and PMMA as $\gamma_{PS-PMMA}$, the wetting pressure can be written as, [22]

$$P = \frac{\gamma_{PS-PMMA}}{a}.$$

The interfacial tension has a temperature dependency, $\gamma_{PS-PMMA}/[mN\cdot m^{-1}] = (3.46 - T/[°C]\cdot 0.013)$ [34]. Consider the smallest PMMA liquid bridge ($a \approx 400$ nm) represented in Fig. 2(a), which yields the highest wetting pressure. At the experimental temperature of 160 °C, $P = 1.7$ kPa, which was orders of magnitude smaller than the external normal pressure in our experiments. To provide a simple thermodynamics argument, we estimate the system Gibbs free energy increase due to pressurization and compare that with the surface/interfacial energy change associated with morphological development. Consider the volume ratio 1:1 between PS and PMMA, when both phases form direct contact with the confining walls, each occupy ½ of the polymer/wall interfacial area. Denoting the thickness, area, interfacial tension of PS/SiO_x, interfacial tension of PMMA/SiO_x, interfacial tension of PS/PMMA as h, A, γ_S, γ_M, $\gamma_{S/M}$, the total interfacial-tension related energy change at both the substrate and superstrate per unit area can be expressed as

$$\Delta E = 2\left(\gamma_S/2 + \gamma_M/2 - \gamma_M - \gamma_{S/M}\right) = \gamma_S - \gamma_M - 2\gamma_{S/M}$$

For the isotropic system with no compositional change, the increase in the system Gibbs free energy per unit area due to pressure increase is

$$\Delta G = \int_{p_0}^{p_0+\Delta p} V dp/A = h\Delta p$$

Plugging in approximated valued from literature [35,36], ΔE was on the order of 2.0×10^{-3} J/m^2 , whereas ΔG was found to be 0.5 J/m^2, differing by 2 orders of magnitude. The effect of pressurization was indeed stronger than the surface/interfacial energy.

Therefore, under external pressure, the coarsening mechanism via wetting layer, as shown by Tanaka, was inhibited (dashed arrow in Fig. 2(e)) and the mass transfer from the wetting layer into the liquid bridge became valid (solid arrow in Fig. 2(e)). Note that the coarsening due to in-plane breakup of PS confined between two neighboring PMMA domains might still occur, and might become increasingly more important as the PMMA domains became larger (PS became more strip/threads like).

Furthermore, we examined the pressurized annealing of varied initial film thickness, and their annealed morphologies are shown in Fig. 3. For all three cases, no phase inversion occurred and no PMMA wetting layer was found in the annealed films, which was consistent with the 134 nm film. The SEM scans (providing larger view than the inset AFM scans) show that the morphology is uniform across the sample surface.

To provide further evidence of pressure-driven inhibition and depletion of the wetting layer, we placed a homogenous PMMA layer atop the PS/PMMA film and examined the effect of compression to the evolution of this layer and the blend film after annealing. The film geometry is schematically shown in Fig. 4(f). Four different PMMA "cushion layer" thicknesses were examined, as labeled on Fig. 4(a–d).

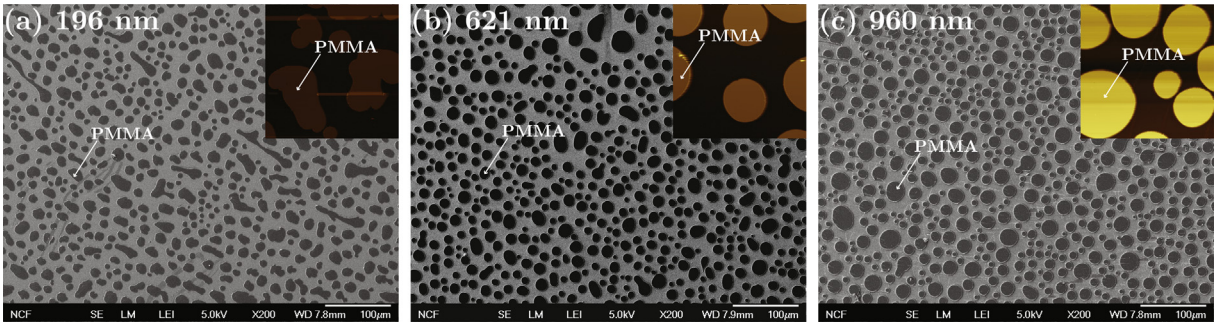

Fig. 3. (a–c) SEM images of PS48k/PMMA15k blend films with the labeled thicknesses after annealing under 4 MPa external normal pressure at 230 °C. PS was selectively removed prior to imaging, allowing for better contrast. Insets are a representative 50 μm × 50 μm AFM scan of the corresponding sample.

Fig. 4(a–d) are the AFM topographic images of the annealed films after selective removal of PS. For all four samples, no wetting layer was observed after the annealing, suggesting that all the PMMA layers had been "squeezed" into the blend films, and more specifically, into the PMMA domains. Both PS and PMMA formed direct contacts with the two substrates. As the PMMA cushion layer thickness increased from 37 nm, to 70 nm, only dispersed PMMA domains within continuous PS phase were observed, and the domain sizes increased. For the 126 nm thick PMMA cushion layer/blend system, PMMA evolved into the matrix phase while PS into dispersed domains (Fig. 4(d)). This was due to the volume fraction of PMMA being the highest in (d). Apparently, all the mass transport from PMMA cushion layers to the blend films had completed by 30 min at 160 °C.

Fig. 4(e) shows the PMMA volume fractions in the annealed blend films (obtained from AFM image analyses) as a function of the PMMA cushion layer thickness. Clearly, for all four systems, the PMMA volume fractions in the annealed blend film matches well with the calculated value (assuming all PMMA cushion layer merged into the final blend films and density remained unchanged). Noticeably, the experimental results are slightly higher than that of the calculated ones, which can be attributed to the overestimation of the actual PMMA domain sizes from the probe-shape convolution in the AFM measurements (since PS had been

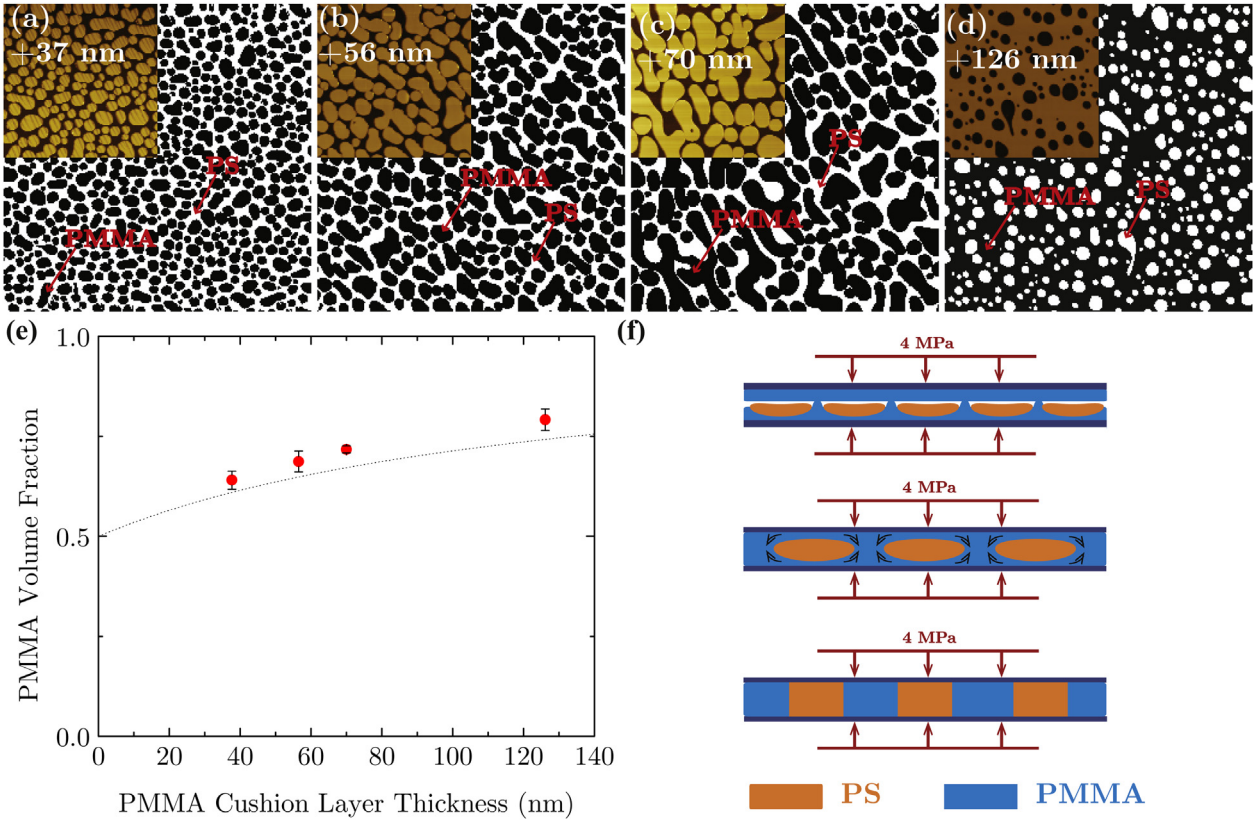

Fig. 4. (a–d) Binarized AFM topographic images of a 134 nm thick PS48k/PMMA15k capped with a spin-cast PMMA cushion layer of the labeled thickness (upper left corner of each image), annealed at 160 °C under 4 MPa vertical pressure for 30 minutes, and subsequently etched with cyclohexane. All images are 50 μm × 50 μm in size. The black areas represent PMMA domains. The insets are the AFM topographic images of the corresponding regions. (e) The PMMA volume fraction measured from the binary images as a function of the PMMA cushion layer thickness. The error bars indicate the statistical standard deviation from 5 different randomly chosen areas. The dotted line is the calculated volume fraction, assuming volume conservation. (f) A schematic illustration of the phase evolution of PS/PMMA blend film annealed while being pressurized against a PMMA cushion layer. The hydrodynamic wetting of PMMA is suppressed and the artificially added cushion layer thins out.

dissolved, and PMMA was always the elevated structure). Clearly, these experiments proved that even relatively thick PMMA "wetting layer" could be squeezed into the originally dispersed domains under a normal pressure that were larger than the hydrodynamic wetting pressure.

4. Conclusions

In summary, we investigated the evolving structures of PS/PMMA blend films under symmetrical confinement with a normal pressure. Silicon wafers with native oxide layers, which preferentially favored PMMA wetting, were used as the capping layers. When no external pressure was exerted on the film, the formation of PMMA wetting layer at the blend–substrate interface was predominant. With the presence of a strong external pressure, the preferential wetting was completely prevented. This was caused by the external pressure counter-balancing the wetting pressure, which drained the PMMA from the wetting layer back into isolated domains. Furthermore, we stacked PMMA homopolymer cushion films of various thicknesses onto the blend film. The cushion films, viewed as an artificially pre-existing "wetting layer", were completely depleted. Therefore, the study showed that pressure could be an effective means to create "neutral wetting" situation for the PS/PMMA films on preferential wetting substrates.

Acknowledgment

The authors acknowledge the funding support from the National Science Foundation under Grant No. CMMI-1031785. We thank Prof. Dean Waldow for kindly providing the ImageJ plug-in that calculates the radially averaged power density spectra.

Appendix A. Supplementary data

Supplementary data related to this article can be found at http://dx.doi.org/10.1016/j.polymer.2014.06.023.

References

[1] Li G, Shrotriya V, Huang J, Yao Y, Moriarty T, Emery K, et al. High-efficiency solution processable polymer photovoltaic cells by self-organization of polymer blends. Nat Mater 2005;4:864–8.
[2] Pommerehne J, Vestweber H, Guss W, Mahrt RF, Bässler H, Porsch M, et al. Efficient two layer leds on a polymer blend basis. Adv Mater 1995;7:551–4.
[3] Liu H, Kameoka J, Czaplewski DA, Craighead HG. Polymeric nanowire chemical sensor. Nano Lett 2004;4:671–5.
[4] Wang H. Ph.D. Dissertation. University of Pennsylvania, Philadelphia, PA, 1999.
[5] Puri S. Surface-directed spinodal decomposition. J Phys Condens Matter 2005;17:R101.
[6] Jones RAL, Norton LJ, Kramer EJ, Bates FS, Wiltzius P. Surface-directed spinodal decomposition. Phys Rev Lett 1991;66:1326–9.
[7] Geoghegan M, Krausch G. Wetting at polymer surfaces and interfaces. Prog Polym Sci 2003;28:261–302.
[8] Binder K. Spinodal decomposition in confined geometry. J Non Equilib Thermodyn 1998;23:1–44.
[9] Straub W, Bruder F, Brenn R, Krausch G, Bielefeldt H, Kirsch A, et al. Transient wetting and 2D spinodal decomposition in a binary polymer blend. EPL Europhys Lett 1995;29:353.
[10] Krausch G, Dai CA, Kramer EJ, Marko JF, Bates FS. Interference of spinodal waves in thin polymer films. Macromolecules 1993;26:5566–71.
[11] Wang H, Composto RJ. Hydrodynamic-flow-driven wetting in thin film polymer blends: growth kinetics and morphology. Phys Rev E 2000;61:1659–63.
[12] Müller M, Albano EV, Binder K. Symmetric polymer blend confined into a film with antisymmetric surfaces: Interplay between wetting behavior and the phase diagram. Phys Rev E 2000;62:5281–95.
[13] Ahn DU, Wang Z, Campbell IP, Stoykovich MP, Ding Y. Morphological evolution of thin PS/PMMA films: effects of surface energy and blend composition. Polymer 2012;53:4187–94.
[14] Wang Z, Ahn DU, Ding Y. Topographically uniform but chemically heterogeneous nanostructures by nanoimprinting demixed polymer blends. Langmuir 2010;26:14909–14.
[15] Wang H, Composto RJ. Thin film polymer blends undergoing phase separation and wetting: Identification of early, intermediate, and late stages. J Chem Phys 2000;113:10386–97.
[16] Wang H, Composto RJ. Wetting and phase separation in polymer blend Films: Identification of four thickness regimes with distinct morphological pathways. Interface Sci 2003;11:237–48.
[17] Binder K, Nielaba P, Pereyra V. Phase coexistence in binary mixtures in thin films with symmetric walls: model calculations for two-and three-dimensional ising lattices. Z Für Phys B Condens Matter 1997;104:81–98.
[18] Wendlandt M, Kerle T, Heuberger M, Klein J. Phase separation in thin films of polymer blends: the influence of symmetric boundary conditions. J Polym Sci Part B Polym Phys 2000;38:831–7.
[19] Tanaka H. Dynamic interplay between phase separation and wetting in a binary mixture confined in a one-dimensional capillary. Phys Rev Lett 1993;70:53–6.
[20] Tanaka H. Wetting dynamics in a confined symmetric binary mixture undergoing phase separation. Phys Rev Lett 1993;70:2770–3.
[21] Tanaka H. Interplay between phase separation and wetting for a polymer mixture confined in a two-dimensional capillary: wetting-induced domain ordering and coarsening. EPL Europhys Lett 1993;24:665.
[22] Tanaka H. Interplay between wetting and phase separation in binary fluid mixtures: roles of hydrodynamics. J Phys Condens Matter 2001;13:4637.
[23] Dalnoki-Veress K, Forrest JA, Dutcher JR. Mechanical confinement effects on the phase separation morphology of polymer blend thin films. Phys Rev E 1998;57:5811–7.
[24] Byun M, Hong SW, Qiu F, Zou Q, Lin Z. Evaporative organization of hierarchically structured polymer blend rings. Macromolecules 2008;41:9312–7.
[25] Mansky P, Liu Y, Huang E, Russell TP, Hawker C. Controlling polymer-surface interactions with random copolymer brushes. Science 1997;275:1458–60.
[26] Winesett DA, Story S, Luning J, Ade H. Tuning substrate surface energies for blends of polystyrene and Poly(methyl methacrylate). Langmuir 2003;19:8526–35.
[27] Han E, Stuen KO, La Y-H, Nealey PF, Gopalan P. Effect of composition of substrate-modifying random copolymers on the orientation of symmetric and asymmetric diblock copolymer domains. Macromolecules 2008;41:9090–7.
[28] Zhang X, Yager KG, Kang S, Fredin NJ, Akgun B, Satija S, et al. Solvent retention in thin spin-coated polystyrene and Poly(methyl methacrylate) homopolymer films studied by neutron reflectometry. Macromolecules 2010;43:1117–23.
[29] Walheim S, Böltau M, Mlynek J, Krausch G, Steiner U. Structure formation via polymer demixing in spin-cast films. Macromolecules 1997;30:4995–5003.
[30] Heriot SY, Jones RAL. An interfacial instability in a transient wetting layer leads to lateral phase separation in thin spin-cast polymer-blend films. Nat Mater 2005;4:782–6.
[31] Walheim S. Ph.D. Dissertation. Konstanz, Germany: Universität Konstanz; 2000.
[32] Zhang Z, Ahn DU, Ding Y. Instabilities of PS/PMMA bilayer patterns with a corrugated surface and interface. Macromolecules 2012;45:1972–81.
[33] Zong Q, Li Z, Xie X. Inversion of phase morphology in polymer-blend thin films on glass substrates. Macromol Chem Phys 2004;205:1116–24.
[34] Mark JE. Physical Properties of Polymers Handbook. 2nd ed. New York: Springer; 2007.
[35] Seemann R, Jacobs K, Blossey R. Polystyrene nanodroplets. J Phys Condens Matter 2001;13:4915.
[36] Wiegand M, Reiche M, Gösele U. Time-Dependent surface properties and wafer bonding of O2-plasma-treated silicon (100) surfaces. J Electrochem Soc 2000;147:2734–40.